ELSEVIER

Biophysical Chemistry 101–102 (2002) 295–307

Biophysical Chemistry

www.elsevier.com/locate/bpc

# Potential of mean force between two hydrophobic solutes in water☆

Noel T. Southall[a], Ken A. Dill[b,*]

[a]*Graduate Group in Biophysics, University of California at San Francisco, San Francisco, CA 94143-1204, USA*
[b]*Department of Pharmaceutical Chemistry, University of California at San Francisco, 3333 California Street, San Francisco, CA 94143-1204, USA*

Received 7 December 2001; accepted 22 February 2002

**Abstract**

We study the potential of mean force between two nonpolar solutes in the Mercedes Benz model of water. Using NPT Monte Carlo simulations, we find that the solute size determines the relative preference of two solute molecules to come into contact ('contact minimum') or to be separated by a single layer of water ('solvent-separated minimum'). Larger solutes more strongly prefer the contacting state, while smaller solutes have more tendency to become solvent-separated, particularly in cold water. The thermal driving forces oscillate with solute separation. Contacts are stabilized by entropy, whereas solvent-separated solute pairing is stabilized by enthalpy. The free energy of interaction for small solutes is well-approximated by scaled-particle theory.


*Keywords:* Hydrophobic interaction; Potential of mean force; Solvent-separated minimum

## 1. Introduction

An underpinning to many fundamental processes in biology and chemistry is the potential of mean force (PMF) between nonpolar molecules in water. The PMF describes the energetics involved when two molecules in a mutual solvent approach each other and interact. It describes desolvation and binding. Examples include the binding of a ligand to a protein or the process by which two parts of a protein chain come together as the protein folds. As a simplest model for this process, there have been several studies of the PMFs between two small nonpolar solutes, as when argon associates with argon or methane associates with methane in water [1–11].

Some studies of hydrophobic association in water involve integrals over the PMFs [12], such as second virial coefficients and related characterizations, which are related to an integrated solute–solute PMF [13–16], or approximation as two thermodynamic states [17,18]. Work of this type

☆ This paper is dedicated to John Schellman, a dear friend and a superb scientist, who has taught us, among many other things, just how subtle the hydrophobic effect can be.

*Corresponding author. Tel.: +1-415-476-9964; fax: +1-415-502-4222.

*E-mail address:* dill@maxwell.ucsf.edu (K.A. Dill).

-/02/$ - see front matter 
PII: -( )-

indicates that association is endothermic at room temperature [17,18,12], and probably has a negative heat capacity of interaction [17,12]. Increasing the temperature enhances the strength of association [12,16].

Such integrated quantities give less microscopic information than would be available if the full PMF were known [5]. Our interest here is in the more detailed structure of the full PMF, and how it depends on temperature and solute size. The PMF between methane molecules in water has been calculated for several systems in recent years [1–11]. Other thermodynamic properties have also been computed, such as entropies [2,5] and heat capacities of interaction [8–10]. An excellent summary is given in Ref. [9].

Our present modeling was undertaken as an extension of such work, in two respects. First, in fully detailed models, it is often challenging to obtain good convergence for the properties that are most relevant to understanding the hydrophobic effect, such as heat capacities and entropies. Second, there has not yet been a systematic study of the effects of solute size and shape. Here we consider the PMF between two hydrophobic solutes using a statistical mechanical model of water that is simple and it is two-dimensional, so we can overcome computational limitations to address these issues.

## 2. Methods

### *2.1. The Mercedes Benz model*

We use the Mercedes Benz (MB) model of water [19], a simple 2D model with water-like properties, originally developed by Ben-Naim [20]. Each MB water molecule is a 2D disk having three hydrogen bonding arms, arranged as in the MB logo. There are two types of interactions between any two water molecules. First, there is a hydrogen bonding interaction that favors the colinear alignment of one arm of one water molecule with one arm of another water. The hydrogen bond energy is a Gaussian function of the distance between the two water centers, and a Gaussian function of the orientation of the hydrogen bonding arms, *i* and *j*, on two different waters with respect to the vector connecting the two water centers, $\vec{u}$:

$$U_{\mathrm{HB}} = \varepsilon_{\mathrm{HB}} \cdot G(r_{ij} - l_{\mathrm{HB}}) \cdot G\left(\vec{i}\cdot\vec{u}_{ij} - 1\right) \cdot G\left(\vec{j}\cdot\vec{u}_{ij} + 1\right) \quad (1)$$

where $G(x) = \exp(-x^2/2\sigma^2)$ is a Gaussian function, the optimal hydrogen bond length is $l_{\mathrm{HB}} = 1$, the optimal hydrogen bond energy is $\varepsilon_{\mathrm{HB}} = -1$, $r_{ij}$ describes the distance between the two molecular centers, and $\sigma = 0.085$. There is no distinction between hydrogen bond donors or acceptors. Hydrogen bonding is strongest when the arms of two different water molecules are pointed directly at each other. The width, $\sigma$, of the Gaussian functions are chosen to be narrow enough to disfavor, but not prevent, the formation of bifurcated hydrogen bonds.

Second, water molecules also interact through a Lennard–Jones (LJ) potential:

$$U_{\mathrm{LJ}}(r_{ij}) = 4\varepsilon_{\mathrm{LJ}}\left(\left(\frac{\sigma_{\mathrm{LJ}}}{r_{ij}}\right)^{12} - \left(\frac{\sigma_{\mathrm{LJ}}}{r_{ij}}\right)^{6}\right) \quad (2)$$

where $\varepsilon_{\mathrm{LJ}}$ and $\sigma_{\mathrm{LJ}}$ are the LJ well-depth and radius. We use $\sigma_{\mathrm{LJ}} = 0.7 l_{\mathrm{HB}}$ and $\varepsilon_{\mathrm{LJ}} = 0.1\varepsilon_{\mathrm{HB}}$.

Nonpolar solutes are modeled as LJ disks that have no hydrogen bonding arms. A nonpolar solute is represented by two parameters, $\sigma_{\mathrm{LJ}}$, which defines the radius of the solute, and $\varepsilon_{\mathrm{LJ}}$, which defines the solute's intermolecular potential with water molecules. Solutes have the same LJ well-depth as the MB waters, $\varepsilon_{\mathrm{LJ}} = 0.1\varepsilon_{\mathrm{HB}}$. For large solutes, the standard Lorentz–Berthelot geometric combining rules [21] give unrealistically broad potentials. To avoid this, we limit $\sigma_{\mathrm{LJ}}$ in the potential to $\sigma_{\mathrm{LJ,max}}$, and offset $r_{ij}$ by the difference,

$$r_{ij} = \begin{cases} r_{ij} & \sigma_{\mathrm{LJ}} \leqslant \sigma_{\mathrm{LJ,max}} \\ r_{ij} - (\sigma_{\mathrm{LJ}} - \sigma_{\mathrm{LJ,max}}) & \sigma_{\mathrm{LJ}} > \sigma_{\mathrm{LJ,max}} \end{cases} \quad (3)$$

where $\sigma_{\mathrm{LJ,max}} = 1.0$.

We perform Monte Carlo simulations on MB water at constant NPT, using periodic boundary conditions and the minimum-image convention. Details can be found elsewhere [19]. In a typical simulation run, 120 MB water molecules were equilibrated with one or two hydrophobic solutes

and statistics were gathered over $10^9$ steps. One step represents an attempted translation or rotation. Simulations were performed at a reduced pressure $P^*=0.19$ ($P^*=k_BT/l_{HB}^2|\varepsilon_{HB}|$) and reduced temperature $T^*=0.21$ ($T^*=k_BT/|\varepsilon_{HB}|$), unless otherwise noted. MB water has its density maximum at $T^*=0.18$, and it undergoes a freezing transition at approximately $T^*=0.16$ [22]. The range of temperatures we explore, as being representative of liquid water, is $0.18\leqslant T^*\leqslant 0.28$. We use a cutoff energy of $0.33\varepsilon_{HB}$ for the purposes of counting numbers of water–water hydrogen bonds. Density plots were generated from statistics on particle center positions, binned over a square grid, step size $0.1l_{HB}$.

The limitations of the MB model are clear: it is 2D, hydrogen bond donors are not distinguished from acceptors, there is no atomic detail or polarizability, and electrostatics is not included. Nevertheless, this model has the virtues that: (1) it is based on a structure-based partition function, (2) because it is 2D, we have less configurational space to sample, which permits good convergence for the subtle properties of interest here, and (3) we believe it captures the essential physics of nonpolar solvation in water, namely LJ attractions and repulsions, and an orientation-dependence that stems from hydrogen bonding. The MB model has previously been shown to qualitatively predict the volume anomalies for pure water—a density minimum, a negative thermal expansion coefficient, and a minimum in the isothermal compressibility. It also predicts the trends for the temperature dependence of the free energy, entropy, enthalpy, heat capacity, and volume change of hydrophobic solute transfer [19,23].

Cavities are areas in solution that have no particle centers within them,

$$U_{\text{HardCavity}}(r_{ij})=\begin{cases}\infty & r_{ij}\leqslant\sigma_{HC}\\ 0 & r_{ij}>\sigma_{HC}\end{cases} \quad (4)$$

where $\sigma_{HC}$ is the sum of radii of two interacting objects. We also compare the behavior of MB water to a hard disk fluid where solvent particles used this same hard potential (Eq. (4)). Hard disk simulations were performed at constant NPT. For the hard disk system, $\sigma_{HC}$ was chosen to have the same value as the LJ size parameter from MB water, $\sigma_{\text{LJ,MB water}}$. The pressure was adjusted so the phase was at the same density as MB water at a given temperature. The hard disk phase is a fluid and has no liquid–vapor phase transition.

### 2.2. Potentials of mean force

Test-particle insertion method (Widom insertion method) and related fluctuation formulas were used to calculate the thermodynamics of association [24,9]. Association is measured as the change in relative to the change in thermodynamics for the infinite dilution case, and as such they are reported as $\Delta\Delta$ quantities. To check convergence, several PMFs were also calculated by umbrella sampling [21]. Both methods yielded very similar results. We show here only the test-particle results. Errors shown in the figures represent one standard deviation of the block averages. Test-particle insertions were attempted into incremental shells, width of $0.04l_{HB}$, around the central solute. We simulate in a bath of 120 MB water molecules, typically for $10^9$ steps, $2\times10^7$ of which were equilibration. Each step was an attempted particle move.

### 2.3. SPT estimation of potentials of mean force

In addition, we use predictions from 2D scaled-particle theory (SPT) [25–28] to predict PMF. SPT can be used to predict the thermodynamics of hard cavity creation in a hard disk fluid, given the density and sizes of the particles. The main result of SPT is a polynomial expression for the free energy of cavity formation, $\Delta G_{\text{cavity}}$, in terms of the cavity radius,

$$\Delta G_{\text{cavity}}=-kT\ln(1-\rho A_1)+kT\left(\frac{2\pi\rho R_1R_2}{1-\rho A_1}\right)+kT\frac{\rho A_2}{(1-\rho A_1)^2} \quad (5)$$

where $k$ is Boltzmann's constant, $T$ is the absolute temperature, $\rho$ is the density of the fluid, $R_1$ and $R_2$ are the radii of particles of type 1 (the solvent) and 2 (the solute), and $A_1$ and $A_2$ are the particle areas, respectively. This utilizes an approximate equation of state for a 2D fluid of hard disks

where the 2D hard disk pressure, $\Pi_{HD}$, is [29]

$$\Pi_{HD} = kT\frac{\rho}{(1-\rho A_1)^2} \quad (6)$$

SPT was first applied to water in 1963 by Pierotti. There are two alternative choices for the pressure that multiplies the volume term in SPT. For the calculation of cavity formation free energies, Pierotti used the ambient pressure [30,31]. Stillinger also used the ambient pressure in modeling cavities in water, since it gives the correct limit for large cavities [32]. Later work used either ambient pressure [33–36] or ignored the pressure term entirely [37–40]. In contrast, here we use the hard disk fluid pressure and surface tension approximated by the equation of state in Eqs. (5) and (6). While it is true that cavity work in MB water becomes dominated by ambient pressure for large cavity sizes, we have found that there is a changeover in the physics: a single SPT-like polynomial expression does not describe both small cavity formation and large cavity formation free energies. Instead, small cavity formation in MB water is more accurately predicted by the hard disk SPT [41].

A PMF reflects how the presence of one solute affects the transfer of another solute into solution. In order to calculate a transfer into an inhomogeneous solution (close to another solute) we assume that SPT can be applied as an integration over a solute's area ($A_2$), and circumference ($C_2$). Our 2D local packing fraction around a solute in MB water is $\phi(\xi)$, where $\xi$ is the distance from the solute. $\phi(\xi)$ is calculated from a convolution of the solvent excluded volume with the simulation solute–water pair distribution function, $\rho(\xi)$. The free energy of cavity formation at a given distance from a solute is

$$\frac{\Delta G_{Cavity}(\xi)}{kT} = -\ln(1-\phi) + \int\left(\frac{\phi(\xi)}{(\pi R_1)(1-\phi(\xi))}\right)dC_2 + \int\left(\frac{\phi(\xi)}{(\pi R_1^2)(1-\phi(\xi))^2}\right)dA_2 \quad (7)$$

and the SPT-estimated PMF is calculated from

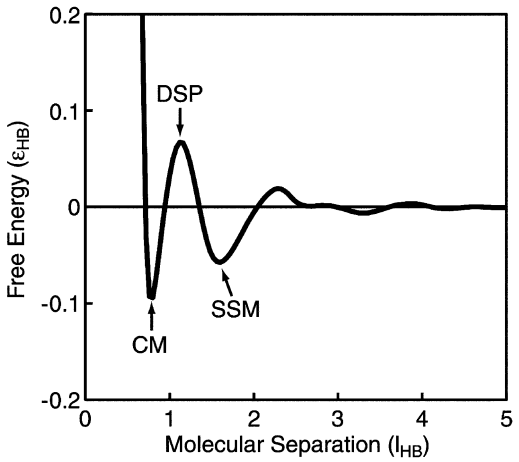


Fig. 1. Solute–solute potential of mean force (PMF) in MB water at $T^* = 0.21$ for solutes, radius $0.7l_{HB}$, showing free energy for the contact minimum (CM), the desolvation peak (DSP), and the solvent-separated minimum (SSM) configurations.

$$\mu_{solute-solute}(\xi) = \Delta G_{cavity}(\xi) - \Delta G_{cavity}(\xi = \infty) + U_{solute-solute}(\xi) \quad (8)$$

A rigorous treatment of $\mu_{solute-solute}$ would utilize $\Delta G_{transfer}$ instead of $\Delta G_{cavity}$. Here we utilize a common approximation: $\Delta G_{transfer} \approx \Delta G_{cavity} + U_{solute-water}$ [31]. However, this approach requires knowledge of $U_{solute-water}(\xi)$ and $U_{solute-water}(\xi = \infty)$. For simplicity, we assume that $U_{solute-water}(\xi) = U_{solute-water}(\xi = \infty)$. Thus, our approximate $\mu_{solute-solute}$ depends only on $\Delta G_{cavity}$.

## 3. Results

### *3.1. Potential of mean force between two small solutes*

We first focus on small solutes. In this case, the two solute molecules have the same LJ parameters as water, and are constructed to model a small atomic solute such as argon [19]. Consistent with a large body of previous work, we find that the PMF for two small hydrophobes in MB water has multiple minima as a function of solute separation (Fig. 1). One stable state is a 'contact minimum' (CM) of the free energy at the solute separation at which the two solutes are in contact ($\approx 0.7l_{HB}$).

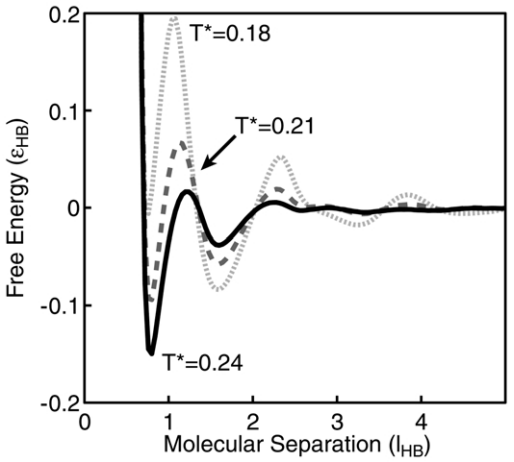


Fig. 2. The free energy of both the CM and the DSP decreases with increasing temperature, while the free energy of the SSM increases. Solute–solute PMF are shown as a function of solution temperature, for $T^*=0.18$ (dotted light grey line), $T^*=0.21$ (dashed dark grey line), and $T^*=0.24$ (solid black line).

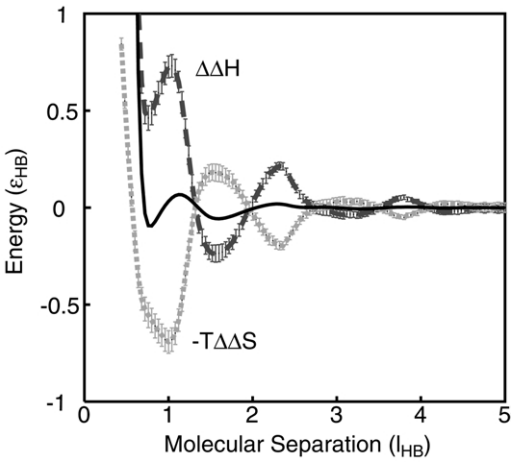


Fig. 3. Apart from the CM, favorable solute–solute configurations are enthalpically favorable, while unfavorable configurations are entropically favorable. Enthalpy of hydrophobic interaction shown in dark grey with error bars, entropy ($-T\Delta\Delta S$) shown in light grey. The solute–solute PMF is shown for reference.

Another stable state is a 'solvent-separated minimum' (SSM) at the solute separation that allows a layer of water between the two solutes. Between these two minima is a free energy maximum, which we call the desolvation peak (DSP) (Fig. 1) [9]. That is, at the DSP the system is unstable, so the solutes will either move to the CM or SSM states. One question of interest, first raised by Pratt and Chandler [42], has been: what are the relative populations of the CM and SSM states? This balance at a given temperature is known to be model-dependent [7,6], but our results are consistent those of other models [3,9] and experiments [16].

Fig. 2 shows the effect of temperature. In cold water ($T^*=0.18$), small solutes have more tendency to be solvent-separated. Increasing the temperature shifts this preference, the contact state becomes more favorable and the solvent-separated state becomes less favorable. At high temperatures ($T^*=0.24$), corresponding to hot liquid water, the contact state is much more populated than the solvent-separated state.

### *3.2. The thermal components of hydrophobic interactions*

The PMF is a free energy as a function of solute separation. What are its entropic and enthalpic

Table 1
Statistics of selected solute configurations compared with the infinitely dilute case at $T^*=0.21$

| Configuration | Distance | $\Delta\langle HB\rangle$ | $\Delta\Delta H(r)$ | $-T\Delta\Delta S(r)$ | $\Delta\Delta C_p(r)$ | $\Delta\Delta G(r)$ |
|---|---|---|---|---|---|---|
| CM | 0.76 | −0.19 | 0.46 | −0.55 | −12 | −0.093 |
| DSP | 1.16 | −0.2 | 0.54 | −0.48 | −3 | 0.066 |
| SSM | 1.60 | 0.06 | −0.24 | 0.18 | 4 | −0.057 |

Shown are the change in average number of hydrogen bonds made per water molecule in the first shell around the solutes ($\Delta\langle HB\rangle$) compared with the enthalpy ($\Delta\Delta H(r)$, in units of $\varepsilon_{HB}$), entropy ($-T\Delta\Delta S(r)$ ($\varepsilon_{HB}$)), heat capacity ($\Delta\Delta C_p(r)$ ($\varepsilon_{HB}/k$)), and free energy of interaction ($\Delta\Delta G(r)$ ($\varepsilon_{HB}$)). Changes in hydrogen bonding correlate strongly with heat capacities, and also with enthalpies and entropies, but not free energies of association.

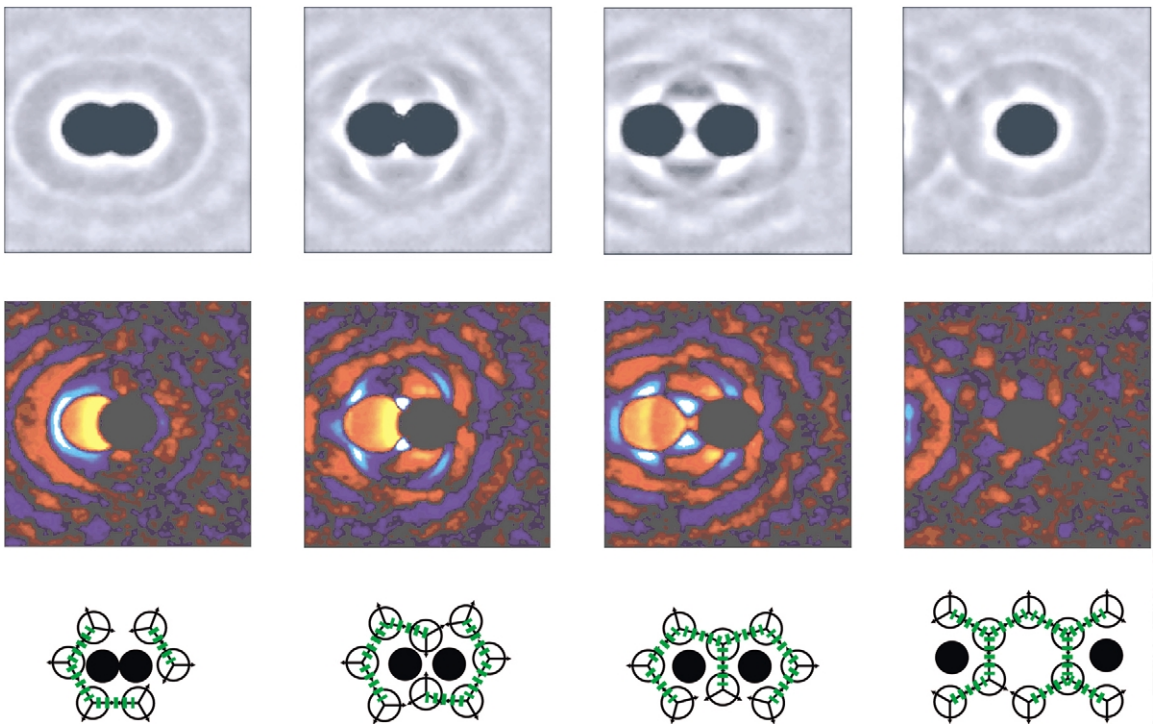

Fig. 4. (*top*) Density of solvent molecule centers around several configurations of solutes over a $5l_{HB} \times 5l_{HB}$ simulation window with solutes at fixed positions, including (from left to right) the CM, DSP, and SSM configurations. Black indicates zero density and white indicates high density regions. CM density is diffuse and radially symmetric, indicating less structure. SSM is highly articulated showing water's preference for particular structures. (*middle*) A difference density map showing how the presence of a second solute perturbs water density versus infinite dilution. Yellow and red indicate density depletion, and blue and white indicate density enrichment and black indicates no change in density. (*bottom*) Idealized 'snapshots' of the first shell of water inferred from simulation data for several configurations of solutes. Green lines suggest formed hydrogen bonds. The CM configuration causes solvent hydrogen bonds to break, while a small enrichment in solvent hydrogen bonding is observed for the SSM state.

components? This was first studied by Smith and Haymet, in a different model [2]. Fig. 3 shows these components in the MB model, as a function of solute separation. We observe an interesting enthalpy–entropy compensation and oscillation. The CM is entropic, consistent with results of Smith and Haymet. The SSM is enthalpic, and solutes separated by one and a half water layers are stabilized by entropy.

This oscillation correlates with hydrogen bonding. Table 1 shows the average count of hydrogen bonds in the three states CM, DSP, and SSM, compared with the enthalpy and entropy components and the heat capacity. When solutes approach the CM, hydrogen bonds are broken, increasing the enthalpy but lowering the entropy, hence this state is entropy-driven. When solutes approach the SSM, it is enthalpically favorable because this state is compatible with adjacent water cages (Fig. 4), resulting in more hydrogen bonding, but lower entropy. The DSP state also breaks hydrogen bonds and is opposed by the enthalpy and favored by the entropy. Fig. 4 shows the solvent density surrounding the two solutes at different separations. Articulated solvent density in the SSM case also indicates hydrogen bond-induced structuring.

An important fingerprint of the hydrophobic effect is the heat capacity. When a nonpolar solute is inserted into water, there is a large positive heat capacity change, $\Delta C_p$. Therefore, according to the traditional view, it follows that when two nonpolar solutes come into contact, the heat capacity change

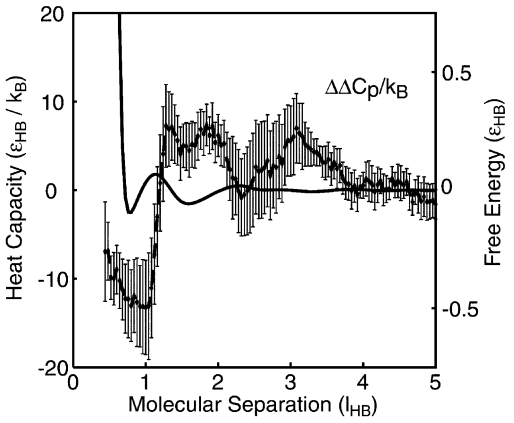


Fig. 5. Heat capacity of hydrophobic interactions as a function of intermolecular separation shown with error bars. The solute–solute PMF is shown for reference. The contact configurations have a negative heat capacity, consistent with several experimental studies.

should be negative. Only recently has it been possible to study, by computer simulation, the heat capacity of the PMF of two nonpolar solutes. So far, the results have been contentious. Shimizu and Chan have found a striking result, namely a small *positive* heat capacity of association for two methanes in TIP4P water [9,10]. Moreover, they found that the DSP has a large *positive* heat capacity, and an *unfavorable* entropy. In contrast, Rick [8]

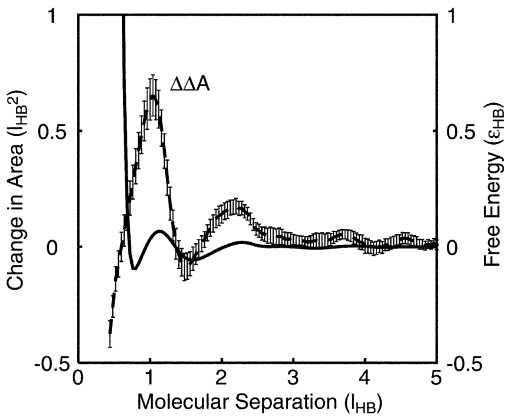


Fig. 6. Area (equivalent to volume in 3D) of hydrophobic interactions as a function of intermolecular separation shown with error bars. The solute–solute PMF is shown for reference. A large DSP barrier is observed.

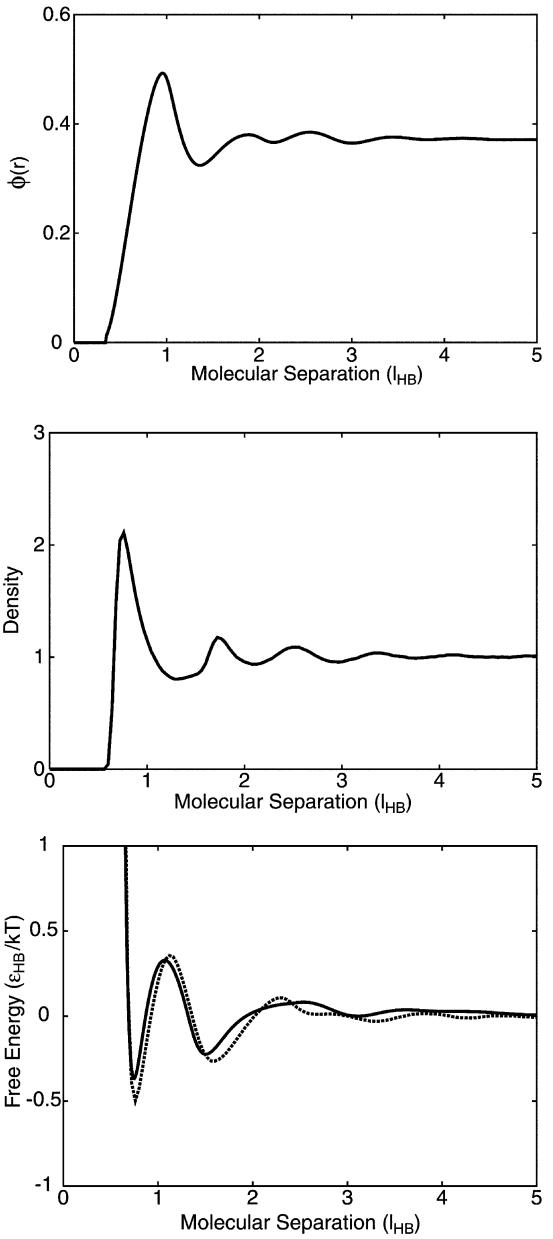


Fig. 7. SPT estimation of solute–solute PMF in MB water. (*top*) Solute–water pair distribution function at infinite dilution in MB water at $T^* = 0.21$, used to calculate the distribution of packing fraction in space. (*middle*) Packing fraction as a function of distance from a single solute, used as input in SPT calculations. (*bottom*) Predicted (solid line) and measured (dotted line) PMF for two solutes in MB water at $T^* = 0.21$.

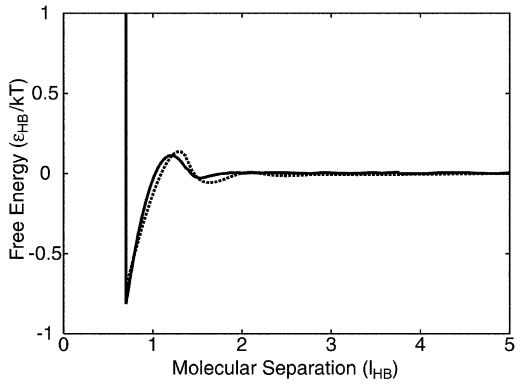


Fig. 8. A hard disk–hard disk PMF from a fluid of hard disks, radius $0.7l_{HB}$, at the density of MB water for $T^*=0.21$ (dotted line) is compared with an iterative SPT prediction (solid line). Discrepancies highlight the approximate nature of the SPT estimate.

reported a negative $\Delta\Delta C_p$ of association, but one that was a puzzling order of magnitude larger than a single methane hydration. The NVT simulations of Ludemann et al. [3] give a negative $\Delta\Delta C_v$.

Our results for $\Delta\Delta C_p(r)$ for the PMF are shown in Fig. 5. We find $\Delta\Delta C_p(r_{CM})<0$ for the CM, consistent with classical expectations, but $\Delta\Delta C_p$ is relatively large and positive for larger solute separations. We find that $\Delta\Delta C_p\approx 0$ at DSP. In short, our negative heat capacities and large positive enthalpies for the CM configuration are consistent with experimental data for hydrophobic association in aqueous solution [17,43]. What is unexpected, however, is the large positive heat capacity for the separated solutes.

Another puzzle has been the pressure dependence of the PMF. One computer simulation study showed that applying pressure, at low pressures, drives solutes into contact because of a positive volume of dissociation, while high pressures had

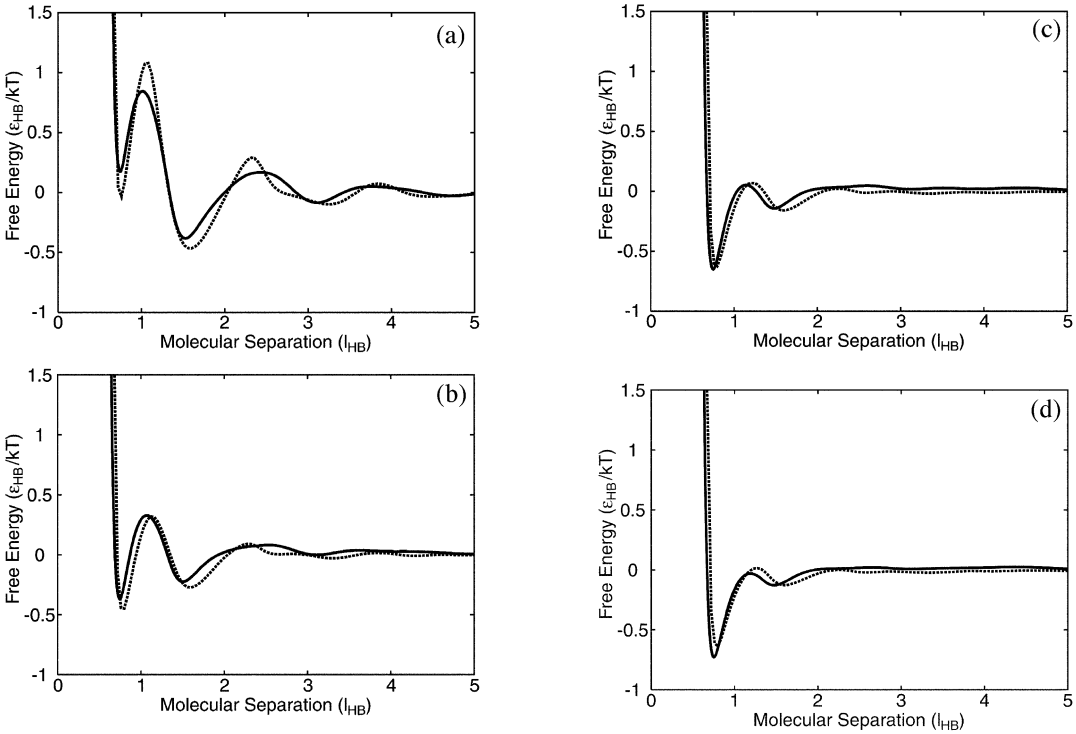


Fig. 9. SPT estimate method predicts accurate temperature dependence of solute–solute PMF in MB water. Shown are results in MB water (a) $T^*=0.18$, (b) $T^*=0.21$, (c) $T^*=0.24$, (d) $T^*=0.26$ for the simulation PMF results (dotted lines) and the SPT estimate (solid lines).

little effect [4]. In contrast, the information theory model predicts a negative volume of dissociation [44], so applied pressure would drive solutes into contact. More recent simulations support the information theory model prediction, but showed that the solvent-separated state was also sensitive to pressure [11]. Other simulations found that the solvent-separated state is the most sensitive to pressure [8].

Fig. 6 shows our results for the area (the 2D analogue of volume in a three-dimensional system) of hydrophobic association for two small hydrophobes. We find that the DSP, the unstable desolvated state, has a large area. It does not fill space efficiently. We also find that the SSM is better-packed than the CM, because of its smaller area. That is, the SSM involves two solutes each surrounded by a water cage, so a water 'fence' separates the two solutes. This state is well-packed. These results are consistent with [11] but not with [4]. The barrier between the two states may explain the kinetic frustration seen in experimental systems as the pressure increases. Increasing pressure slows protein folding kinetics [45,46], in a way that mimics its effect on hydrophobic interactions [44,8,11].

### *3.3. The free energies are described by the hard disk model*

We have noted that the entropy, enthalpy, and heat capacity of association correlate with first-shell-water hydrogen bonding. However, because of enthalpy–entropy compensation, the free energy: (1) is much smaller than the entropy or enthalpy components, (2) is sensitive to parameters of the model [7,6], and (3) in our simulations, does not correlate with first-shell hydrogen bonding.

It raises the question of whether the PMF of MB water might be captured by simpler models. The oscillation in the PMF between solutes in a fluid generally reflects the particulate nature of the solvent [42,47,48]. The most favorable potentials between two hydrophobes occur at the distances where the solvent number density is largest (Fig. 7a). This is due to excluded volume. Even in simple hard disk fluids, solutes prefer to be at the

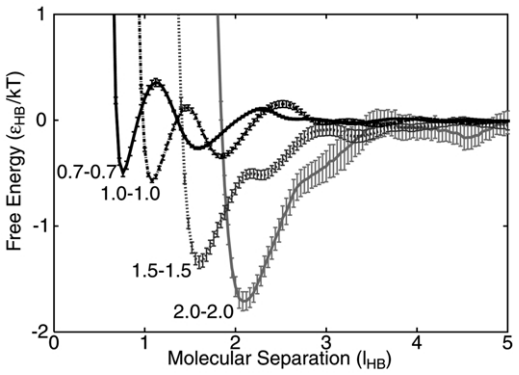


Fig. 10. Solute size dependence of PMF in MB water. Four experiments are shown with error bars, PMFs at $T^*=0.21$ for pairs of $0.7l_{HB}$, $1.0l_{HB}$, $1.5l_{HB}$ and $2.0l_{HB}$ solutes. Large solutes have very deep and favorable CM, consistent with the idea that burial of hydrophobic surface is favorable for large solutes.

CM or SSM (Fig. 8), so these preferred states do not arise because of special features of water.

We apply SPT as follows. From our Monte Carlo simulations, we obtain a solute–water pair distribution function, as shown in Fig. 7a. From that, we obtain the solvent packing fraction $\phi(r)$ as a function of distance $r$ from the solute (Fig. 7b). This quantity is then put into the SPT machinery to calculate the free energy of cavity formation for a new cavity at a given distance from the solute, $\Delta G_{\text{cavity}}(r)$ (Fig. 7c). To get the PMF, we calculate the free energy of cavity formation at a given distance from the solute using SPT and subtract from it the free energy of forming a cavity in bulk water. The contribution of the solute–water interaction energy is ignored. It is assumed that this energy largely cancels with the solute–water interaction energy in the bulk case.

The accuracy of using an integrated form of SPT can be assessed by calculating the pdf of hard disks. This can be determined with the SPT method by an approximate iterative approach where each cycle's input solute–solvent pdf uses the output solute–solute PMF from the previous cycle, which works because there is no distinction between solutes and solvent and SPT provides a very accurate estimate of hard disk transfer. As an initial guess for the packing fraction, we start with a flat

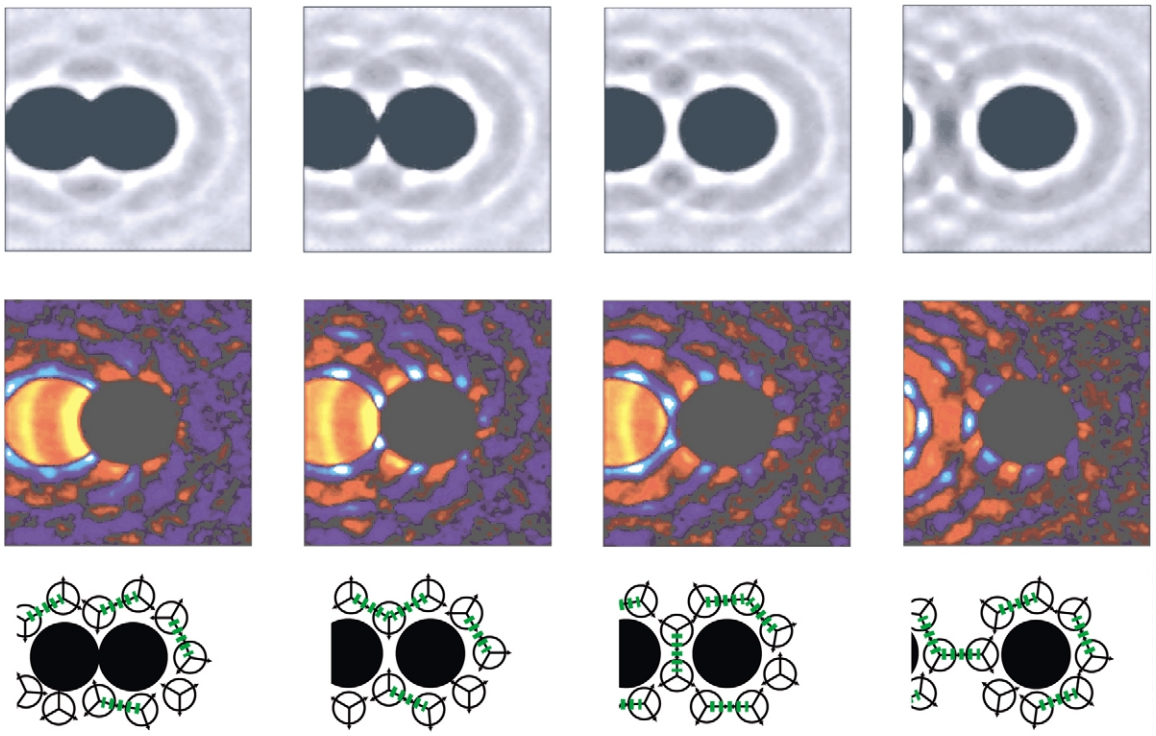

Fig. 11. (*top*) Density of solvent molecule centers around several configurations of larger ($1.5l_{HB}$) solutes over a $5l_{HB}\times5l_{HB}$ simulation window with solutes at fixed positions, including the CM, DSP, and SSM configurations. Black indicates zero density and white indicates high density regions. (*middle*) A difference density map showing how the presence of a second solute perturbs water density versus infinite dilution. Yellow and red indicate density depletion, blue and white indicate density enrichment, and black indicates no change in density. (*bottom*) Idealized 'snapshots' of the first shell of water inferred from simulation data for several configurations of solutes. Green lines suggest formed hydrogen bonds. The transition from SSM to CM clearly results in fewer total number of shell waters for the solutes shown. For all of these configurations first shell waters have more broken hydrogen bonds than bulk waters.

pair distribution function. The converged result after many iterations is shown in Fig. 8.

The SPT approximate approach reproduces the full temperature dependence of the solute–solute PMF in MB water (Fig. 9). As water density in the first shell decreases with increasing temperature, it becomes easier to transfer another solute into the first shell. As water density becomes increasingly homogenous in the outer shells with increasing temperature, the DSP and SSM become less pronounced.

So, what is the role of hydrogen bonding in MB water? The structure of water determines the packing fraction around a solute, $\phi(r)$. The success of SPT indicates that cavity formation energy costs, either adjacent to a solute or in bulk solvent, are largely equivalent to those of opening a cavity in simpler fluids. But water structure impacts this in several ways. First, MB waters have longer-ranged correlations than hard disk fluids. So hydrophobic interactions in the MB model occur over longer distances. Second, water structuring melts out with increasing temperature, as the system temperature is raised, so hydrophobic interactions in the MB model approach those of hard disk PMFs. Third, rising temperatures have different effects on the CM and the SSM, reflecting the changes in water densities around solutes with increasing temperature. As the density of water in contact with a solute decreases with increasing temperatures, the

CM becomes more favorable. As the density of second shell water flattens out, so does the SSM. Hydrogen bonding and the structure of liquid water play important roles in hydrophobic interactions, particularly in the entropy, enthalpy, and heat capacity of interaction, but they affect the free energy of interaction only insofar as $\phi(r)$ is affected.

### *3.4. Hydrophobic interactions depend on solute size*

Finally, we have also studied the effects of solute size on the PMF. Fig. 10 shows that while the SSM state is relatively populated for small solutes, it becomes less important with increasing solute size. Previous work showed that large, flat surfaces cause hydrogen bonds to break between interfacial waters. Here we show that the burial of such hydrophobic surface leads to very favorable free energies at contact for solutes. From the density plots for several configurations of large solutes (Fig. 11) we see that bringing the two solutes into contact reduces the average number of high energy waters at the surface of these molecules. The large variability in PMF's between small and large solutes was predicted to have important implications for complex systems like proteins, and their folding pathways [49]. Here we observe that these different length scales systems do exhibit very different behavior.

## 4. Conclusion

By computer simulations, we study how two nonpolar solutes interact with each other in the MB model of water. According to the simple classical picture, transferring a nonpolar solute into water is characterized by: a large opposing entropy in cold water, a large opposing enthalpy in hot water, hence a large positive heat capacity of transfer, and tighter packing because of the constriction of waters around the solute. Therefore, when two solutes come together in water, it would be expected to lead to a favorable entropy of contact in cold water, a favorable enthalpy in hot water, a negative heat capacity of association, and less dense packing, relative to the state in which the solutes are highly separated in water. Our results for the CM are compatible with this picture for spherical solutes that are small, approximately the diameter of water or smaller. And we find that the free energies embodied in the PMF are well-approximated by the hard disk model of fluids in SPT.

However, this picture does not tell the whole story about the process by which two nonpolar solutes come into contact in water. (1) For small solutes, there is also a relatively stable SSM, which is *enthalpy*-driven and has a *large positive* heat capacity of association. This state involves *making* hydrogen bonds in the solvation shell, at high temperatures, rather than breaking them. (2) The balance between the SSM and CM shifts toward the CM with increasing solute size.

## References

[1] K. Watanabe, H.C. Andersen, Molecular dynamics study of the hydrophobic interaction in aqueous solution of krypton, J. Phys. Chem. 90 (1986) 795–802.
[2] D.E. Smith, A.D.J. Haymet, Free energy, entropy, and internal energy of hydrophobic interactions: computer simulations, J. Chem. Phys. 98 (8) (1993) 6445–6454.
[3] S. Ludemann, H. Schreiber, R. Abseher, O. Steinhauser, The influence of temperature on pairwise hydrophobic interactions of methane-like particles, J. Chem. Phys. 104 (1) (1996) 286–295.
[4] V.A. Payne, N. Matubayasi, L.R. Murphy, R.M. Levy, Monte Carlo study of the effect of pressure on hydrophobic association, J. Phys. Chem. B 101 (1997) 2054–2060.
[5] S. Ludemann, R. Abseher, H. Schreiber, O. Steinhauser, The temperature-dependence of hydrophobic association in water. Pair versus bulk hydrophobic interactions, J. Am. Chem. Soc. 119 (18) (1997) 4206–4213.
[6] W.S. Young, C.L. Brooks, A reexamination of the hydrophobic effect: exploring the role of the solvent model in computing the methane–methane potential of mean force, J. Chem. Phys. 106 (22) (1997) 9265–9269.
[7] J.A. Rank, D. Baker, Contributions of solvent–solvent hydrogen bonding and van der Waals interactions to the attraction between methane molecules in water, Biophys. Chem. 71 (1998) 199–204.
[8] S.W. Rick, Free energy, entropy and heat capacity of the hydrophobic interaction as a function of pressure, J. Phys. Chem. B 104 (29) (2000) 6884–6888.
[9] S. Shimizu, H.S. Chan, Temperature dependence of hydrophobic interactions: a mean force perspective, effects of water density, and nonadditivity of thermo-

dynamics signatures, J. Chem. Phys. 113 (11) (2000) 4683–4700.
[10] S. Shimizu, H.S. Chan, Configuration-dependent heat capacity of pairwise hydrophobin interactions, J. Am. Chem. Soc. 123 (9) (2001) 2083–2084.
[11] T. Ghosh, A.E. García, S. Garde, Molecular dynamics simulations of pressure effect on hydrophobic interactions, J. Am. Chem. Soc. 123 (44) (2001) 10997–11003.
[12] H.A. Sheraga, Theory of hydrophobic interactions, J. Biomol. Struct. Dyn. 16 (2) (1998) 447–460.
[13] E.E. Tucker, S.D. Christian, Prototype hydrophobic interaction—dimerization of benzene in water, J. Phys. Chem. 83 (3) (1979) 426–427.
[14] E.E. Tucker, E.H. Lane, S.D. Christian, Vapor-pressure studies of hydrophobic interactions—formation of benzene–benzene and cyclohexane–cyclohexanol dimers in dilute aqueous-solution, J. Sol. Chem. 10 (1) (1981) 1–20.
[15] R.P. Kennan, G.L. Pollack, Pressure dependence of the solubility of nitrogen, argon, krypton, and xenon in water, J. Chem. Phys. 93 (4) (1990) 2724–2735.
[16] M. Mayele, M. Holz, A. Sacco, NMR studies on hydrophobic interactions in solution, Phys. Chem. Chem. Phys. 1 (1999) 4615–4618.
[17] S.D. Christian, E.E. Tucker, Importance of heat capacity effects in the association of hydrocarbon moieties in aqueous solution, J. Sol. Chem. 11 (10) (1982) 749–754.
[18] D. Hallen, I. Wadso, D.J. Wasserman, C.H. Robert, S.J. Gill, Enthalpy of dimerization of benzene in water, J. Phys. Chem. 92 (12) (1988) 3623–3625.
[19] K.A.T. Silverstein, A.D.J. Haymet, K.A. Dill, A simple model of water and the hydrophobic effect, J. Am. Chem. Soc. 120 (13) (1998) 3166–3175.
[20] A. Ben-Naim, Statistical mechanics of 'waterlike' particles in two dimensions. I. Physical model and application of the Percus–Yevick equation, J. Chem. Phys. 54 (9) (1971) 3682–3695.
[21] M.P. Allen, D.J. Tildesley, Computer Simulation of Liquids, Oxford University Press, Oxford, 1987.
[22] K.A.T. Silverstein, K.A. Dill, A.D.J. Haymet, Hydrophobicity in a simple model of water: solvation and hydrogen bond energies, Fluid Phase Equilibria 150 (1998) 83–90.
[23] N.T. Southall, K.A. Dill, The mechanism of hydrophobic solvation depends on solute radius, J. Phys. Chem. B 104 (6) (2000) 1326–1331.
[24] P.E. Smith, Computer simulation of cosolvent effects on hydrophobic hydration, J. Phys. Chem. B 103 (3) (1999) 525–534.
[25] H. Reiss, H.L. Frisch, J.L. Lebowitz, Statistical mechanics of rigid spheres, J. Chem. Phys. 31 (1959) 369.
[26] E. Helfand, H.L. Frisch, J.L. Lebowitz, Theory of the two- and one-dimensional rigid sphere fluids, J. Chem. Phys. 34 (3) (1961) 1037–1042.
[27] R.C. Chatlier, A.P. Minton, Adsorption of globular proteins on locally planar surfaces, Biophys. J. 71 (1996) 2367–2374.
[28] J. Talbot, Molecular thermodynamics of binary mixture adsorption: a scaled particle theory approach, J. Chem. Phys. 106 (11) (1997) 4696–4706.
[29] T. Boublik, 2-dimensional convex particle liquid, Mol. Phys. 29 (2) (1975) 421–428.
[30] R.A. Pierotti, The solubility of gases in liquids, J. Phys. Chem. 67 (1963) 1840–1845.
[31] R.A. Pierotti, Aqueous solutions of nonpolar gases, J. Phys. Chem. 69 (1) (1965) 281–288.
[32] F.H. Stillinger, Structure in aqueous solutions of nonpolar solutes from the standpoint of scaled-particle theory, J. Sol. Chem. 2 (2) (1973) 141–157.
[33] A. Pohorille, L.R. Pratt, Cavities in molecular liquids and the theory of hydrophobic solubilities, J. Am. Chem. Soc. 112 (1990) 5066–5074.
[34] L.R. Pratt, A. Pohorille, Theory of hydrophobicity: transient cavities in molecular liquids, Proc. Natl. Acad. Sci. USA 89 (1992) 2995–2999.
[35] F.M. Floris, M. Selmi, A. Tani, J. Tomasi, Free energy and entropy for inserting cavities in water. Comparison of Monte Carlo simulation and scaled particle theory results, J. Chem. Phys. 107 (16) (1997) 6353–6365.
[36] N. Matubayasi, M. Nakahara, Super- and subcritical hydration of nonpolar solutes. I. Thermodynamics of hydration, J. Chem. Phys. 112 (18) (2000) 8089–8109.
[37] M. Lucas, Size effect in transfer of nonpolar solutes from gas or solvent to another solvent with a view on hydrophobic behavior, J. Phys. Chem. 80 (4) (1976) 359–362.
[38] J.P.M. Postma, H.J.C. Berendsen, J.R. Haak, Thermodynamics of cavity formation in water, Faraday Symp. Chem. Soc. 17 (1982) 55–67.
[39] R.M. Jackson, M.J.E. Sternberg, Application of scaled particle theory to model the hydrophobic effect: implications for molecular association and protein stability, Protein Eng. 7 (3) (1994) 371–383.
[40] I. Tomas-Oliveira, S. Wodak, Thermodynamics of cavity formation in water and *n*-hexane using the widom particle insertion method, J. Chem. Phys. 111 (18) (1999) 8576–8587.
[41] N.T. Southall, Insights on the hydrophobic effect in a simple model of water. PhD Thesis, Graduate group in Biophysics, Univ. Ca., San Francisco, 2001.
[42] L.R. Pratt, D. Chandler, Theory of the hydrophobic effect, J. Chem. Phys. 67 (1977) 3683–3704.
[43] H.A. Scheraga, Theory of hydrophobic interactions, J. Biomol. Struct. Dyn. 16 (2) (1998) 447–460.
[44] G. Hummer, S. Garde, A.E. García, M.E. Paulaitis, L.R. Pratt, The pressure dependence of hydrophobic interactions is consistent with the observed pressure denaturation of proteins, Proc. Natl. Acad. Sci. USA 95 (1998) 1552–1555.
[45] G.J.A. Vidugiras, J.L. Markley, C.A. Royer, Evidence for a molten globule-like transition state in protein

folding for determination of activation volumes, Biochemistry 34 (15) (1995) 4909–4912.
[46] M.M.C. Sun, N. Tolliday, C. Vetriani, F.T. Robb, D.S. Clark, Pressure-induced thermostabilization of glutamate dehydrogenase from the hyperthermophile Pyrococcus furiosus, Prot. Sci. 8 (1999) 1056–1063.
[47] C. Pangali, M. Rao, B.J. Berne, A Monte Carlo simulation of the hydrophobic interaction, J. Chem. Phys. 71 (7) (1979) 2975–2981.
[48] G. Ravishanker, M. Mezei, D.L. Beveridge, Monte Carlo computer simulation study of the hydrophobic effect: potential of mean force for $[(CH_4)_2]$aq at 25 and 50 deg C, Faraday Symp. Chem. Soc. 17 (1982) 79–91.
[49] K. Lum, D. Chandler, J.D. Weeks, Hydrophobicity at small and large length scales, J. Phys. Chem. B 103 (22) (1999) 4570–4577.